

A novel U-shaped acoustic-manipulated design to enhance the performance of low-efficiency filters for sub-micron particles

Y.T. Zhang¹, S.K. Lai^{1,*}, Jerry C.W. Yu¹, H. Guo¹ and C.W. Lim²

¹*Department of Civil and Environmental Engineering, The Hong Kong Polytechnic University, Kowloon, Hong Kong, P.R. China*

²*Department of Architecture and Civil Engineering, City University of Hong Kong, Kowloon, Hong Kong, P.R. China*

Abstract

Acoustic manipulation is a non-contact process that applies acoustic waves to immobilize particles into a specific region for a variety of potential applications. This provides an alternative way to address air ventilation requirements where building systems are becoming smarter and more efficient. Development of such a process within confined spaces can incorporate microscopic interactions to filter aerosol-based particulate matter (PM). In real-engineering conditions, it is hard to filter sub-micron particles (0.25–1.0 μm) than super-micron particles ($> 2.5 \mu\text{m}$) by using low-grade filters. The objectives of this work are twofold. First, we propose a new acoustic-driven pre-filtering device (i.e., a U-shaped resonant acoustic chamber) that can improve the working efficiency of low-grade filters for capturing such particles. Second, the device can optimize spatial homogeneity to enhance the removal efficiency of airborne particles under lower sound intensity requirements. The U-shaped acoustic-driven device in the form of a resonant chamber allows PM to reside at the pressure node of a standing wave. **Experimental studies are conducted to verify the present design. The results show that an overall filtration efficiency of up to 89% for 1.0- μm airborne particles can be achieved when the acoustic-driven device is coupled together with a low-grade MERV-6 coarse filter.** As a standalone device, the acoustic effect works well for the sub-micron particles with a filtration efficiency of up to 61% under a lower sound pressure level (116 dB) than as previously reported in the literature. In the analysis, we also discuss the performance dependence on frequency, sound pressure level and flow rate in terms of particle size distribution. The relevance of this research is a major step towards engineering an acoustic-based pre-filtering technique for developing future innovative ventilation solutions.

Keywords: Mechanical ventilation, Particle trapping, Particulate matter, Filtration efficiency

*Corresponding author. E-mail address: sk.lai@polyu.edu.hk

1. Introduction

Explosive population growth and the dynamic shift in urban sprawl pose great challenges in air pollution. Significant changes in housing needs for large populations have led to a substantial increase in the construction of high-rise dwellings, which have stringent air quality requirements. Poor-quality indoor air affects the lives of many people who live in urban environments. Indoor air quality is thus a crucial issue that deserves greater concern, particularly because public awareness of pollution is dramatically changing people's views towards their health. Fine aerosol particles smaller than $1.0\ \mu\text{m}$ may cause significant respiratory problems that lead to rising health costs and widespread societal losses [1]. To maintain good indoor air quality and thermal comfort, heating, ventilation and air-conditioning (HVAC) systems in buildings, in either mixing, downward or displacement form, play an important role in providing sufficient fresh air exchanges and reducing exposure to outdoor particles. Although outdoor and indoor air pollutants interact via building envelopes and ventilation systems [2], the degradation of indoor air quality may be worse than that of outdoors because contained areas can catalyze the accumulation of potential pollutants.

Epidemiological evidence has shown that a good ventilation practice is recognized as a means of reducing the possibility of airborne viral transmission in confined indoor spaces and associating with the decreased risk of viral infection transmission [3, 4]. Viruses can spread through the air on dust, fibers, and other microscopic particles because air is the primary carrier of contaminants and airborne particulates in buildings [5, 6]. HVAC systems have been proposed to maintain a healthy environment in commercial offices and hospital wards not only by providing thermal comfort to the occupants but also by improving resistance to infection [7, 8]. It is plausible that infectious viruses carried by airborne PM can be disseminated throughout buildings via the air recirculation of HVAC systems [3]. Hence, the development of advanced technologies to improve ventilation and filtration needs is of great research interest.

Various air-filtering technologies [9, 10] have been adopted in high-rise buildings. Low-grade filters (e.g., minimum efficiency rating value (MERV) of 6–9) are generally installed inside air ventilation ductworks. However, they are not effective for capturing fine or ultrafine particles at a sub-micrometer scale. Indeed, two of the most common approaches involve electrostatic diffusion or staining impingement methods. Filters that remove coarse particles larger than $2.5\ \mu\text{m}$ are often used in building ventilation. These are typically made of an activated carbon air-filter medium, a polyurethane foam air-filter, and polyester impingement materials. The use of high-efficiency

particulate air (HEPA) filters is a promising way to achieve better capturing efficiency, however this inevitably reduces the maximum airflow rate, which must be offset by greater extraction fan power in a ventilation system. HEPA filters must also be replaced frequently, as they become ineffective beyond their lifetime to result in a polluted environment. The capital and replacement costs of HEPA filters are thus higher. Hence, there is a need for an innovative device not only to effectively remove fine particles from indoor air, and also to meet long-term sustainability targets [1] and environmental regulations [11].

It is known that acoustic trapping is an active but contact-free manipulation technique under research of capturing particles (e.g., aerosols, dust, and hazardous objects) in a fluid flow [12, 13]. By achieving a standing wave field, fine particles can be forced to reside and trapped into a specific zone/region, which can enhance a filtering function. Furthermore, as particulates accumulate, the use of acoustic pressure prompts these particulates to form larger structures by collision and adhere them together, i.e., acoustic agglomeration. In the literature, Temkin [14] and Hoffmann [15] defined it as an orthokinetic and aerodynamic process in which particle coalescence is induced by an acoustic wave [16]. Sarabia et al. [17] performed a thorough investigation of the ultrasonic agglomeration of micron-sized aerosol particles by a high-intensity standing wave. Fu et al. [18] developed a numerical model based on the lattice Boltzmann equation to study particle coagulation processes under acoustic effects. Liu and Li [19] found agreement between their experimental results and a simulation of acoustic agglomeration via computational strategies. Shi et al. [20, 21] proposed a three-dimensional computational fluid dynamics–discrete element model to investigate the efficiency of acoustic agglomeration on sprayed liquid droplets. Zheng et al. [22] further studied acoustic agglomeration of fine particles in the device based on coupling population balance model to illustrate the particle collision process.

A series of independent experiments have also examined the acoustic force of smoke and aerosols [23-25] in various engineering applications. These studies showed that acoustic agglomeration can be achieved by sound pressure fields, via acoustic streaming and acoustic radiation force. Specifically, Yuen et al. [26-28] used a numerical model and experimental validation to investigate ultrasonic agglomeration, using a mechanical transducer for aerosol removal. In addition, they determined the efficiency of particle removal by varying the inputs, initial concentrations, and size distributions of the aerosol particles. The ultrasonic mechanism was implemented via compressed air using a 28.5-kHz sound wave of greater than 138 dB. Ng et al. [16] used an acoustic agglomeration pre-conditioning

device operating at 6.4 kHz and 140 dB in a ventilation system to enhance the efficiency of filtration of PM_{2.5}. Shi et al. [29] constructed a resonant structure for the removal of fine particles with sound pressure levels (SPLs) greater than 145 dB and frequencies between 400 and 2000 Hz. Qiao et al. [30, 31] applied fine particle manipulation with a two-dimensional acoustic standing field emitted by two pairs of Helmholtz resonators at greater than 130 dB, and observed that aerosols could be manipulated by multiple acoustic-wave packets under a resonant condition. In practice, 15–30% of the energy consumption would be generally applied to air distribution by mechanical-driven fans to overcome pressure drop in ventilation ducts and across filters in building systems [16]. Hence, a combination of acoustic-driven pre-filtering techniques and commercial coarse filters should be a promising way to enhance filtration efficiency and simultaneously maintain a relatively unobstructed flow condition.

The aforementioned studies demonstrated significant achievements under high SPLs (i.e., 130–140 dB). However, the problem of high SPLs is a potential barrier to restrict the application of acoustic-driven techniques in actual building scenes. Hence, a further study and notable breakthrough, to improve the removal efficiency of airborne fine particles (especially for sub-micron particles) under lower SPLs, is of current focus. Using the concept of “acoustic trapping”, we develop a simple U-shaped device (i.e., double resonant acoustic chambers) that can work at lower SPLs to enhance the filtration efficiency of sub-micron particles by using low-grade filters. This technique is based on a unique airflow configuration (i.e., fluid flows in the device are in parallel, but sound waves are in opposite directions) in a ventilation duct. **In this study, we conduct both numerical analysis and experimental study, in which numerical analysis aims to offer design guidelines for the preparation and fabrication of experimental work, such as the working conditions of loudspeakers and the dimensions of the U-shaped device. In the experimental part, a testing prototype is assembled to verify the filtration efficiency of sub-micron particles in the presence of acoustic waves.** Furthermore, we show that a high filtration efficiency can be achieved as the acoustic-driven technique is used along with a commercial MERV-grade filter. We discuss in depth how the PM filtration can be achieved by the acoustic-based pre-filter, as described in the subsequent sections.

2. Theoretical Analysis and Experimental Studies

2.1 Working Principle

To understand the operating principles of acoustic-driven techniques, the basis of acoustic-particle interactions is briefly reviewed in Sections 2.1.1–2.1.3. Using such techniques, it is generally achieved by the generation of a one-dimensional standing wave field in a medium, which can create

differential pressure regions. Due to the pressure gradient, moving particles can be trapped at pressure nodes, where can strengthen the microscopic interaction of particles.

2.1.1 Design of Enclosure Configuration

Fig.1 shows two schematic diagrams of acoustic-driven configurations. Fig. 1(a) is a common design with high intensity acoustic-based particle treatments with a loudspeaker mounted at the top of a ventilation duct. Particles within the airflow appear to coincide with the flow fields. This case requires a high-intensity acoustic energy to force the particles gathering, as the moving direction of such particles is perpendicular to acoustic waves [16, 26, 28-31]. However, in this configuration, the acoustic energy is dispersed in the whole ventilation duct, as no physical boundary is present to concentrate the emitted sound waves. We have observed this by identifying the angular spread in the numerical simulations of our previous work [32].

In this research, we propose a novel configuration as shown in Fig. 1(b). A confined chamber to facilitate particle trapping is designed, in which acoustic waves emitted from a loudspeaker is in an opposite direction against an incoming airflow. The present acoustic resonant chamber with incoming airflow enables a better utilization of sound energy, which can be verified via the numerical simulation of particle trajectories in Section 3. The resonant acoustic chamber forms a one-dimensional standing wave to create acoustic pressure nodes at a specific region. This forces the sound waves propagating in one dimension, and thus effectively minimizes the spread of sound waves from the loudspeaker source. Airborne particles moving inside the resonance tube can be captured by the pressure nodes by using the full extent of the enclosure without dispersing the sound pressure fields. The above two design approaches illustrate how different geometries and speaker locations can affect the residence time effect of airborne particles under sound pressure fields. In the present design configuration, the emitted sound waves are confined and reflected off the hard boundary walls of the chamber. It is thus favorable to induce a trapping region at lower SPLs to enhance utilization of sound energy for particle treatment as a pre-filtering technique.

2.1.2 Resonant Frequency in a Fixed Enclosure

Studies of the mechanisms of acoustic-particle interaction have been identified by numerical methods. For example, Zhang et al. [33] investigated a three-dimensional discrete element model of the acoustic agglomeration of sprayed aerosol droplets that considered orthokinetic interaction, the acoustic wake effect, gravity force, and the Brownian random force. Liu and Li [19] implemented a

parallel computing strategy that included acoustic particle interaction mechanisms and a particle collision process, which allowed prediction of the trapping rate with consideration of varying influencing factors.

In contrast, another study investigated acoustic agglomeration parameters using a theoretical model to facilitate the acoustic agglomeration of PM10 [32]. This study identified the initial conditions, such as the acoustic wave-spread angle, frequency, SPL, and particle trajectory under the influence of an acoustic radiation force. Using a tube enclosure with a cross-section of 15 cm and a flow rate of 0.1–0.3 m/s at an SPL of 160 dB, incoming particles can be captured along an acoustic field [32], where an SPL of 145–165 dB was examined in Refs. [29, 34] before. Particles gathering can be observed when the resonant frequencies emitted from the loudspeaker corresponds to the dimensions of the enclosure, which is a ventilation tube model. This requires a reflective sound panel to be placed on the wall opposite to the loudspeaker, and the corresponding resonant frequencies thus depend on the geometry of the tube.

Consider the present design as a closed tube at both ends, the acoustic frequency can be calculated as follows:

$$f = \frac{mc}{2L}, \quad m = 1, 2, 3... \quad (1)$$

where f is the frequency in Hz, c is the speed of sound in air (= 343 m/s), L is the length of the resonant chamber, and m is the harmonic order number of the emitted frequency. As a finite number of harmonics can be generated using this tube system to form a standing wave, the wavelength λ may be tuned to various harmonic orders. **In general, acoustic pressure (i.e., the force of sound exerting on a surface area) is the main quantity to characterize acoustic fields. In this study, the acoustic pressure model is simplified as a two-dimensional (2D) acoustic enclosure driven at a constant frequency and same phase. To determine the effect of acoustic intensity, we define “SPL” as the following standard logarithmic form**

$$\text{SPL} = 20 \log_{10} \left(\frac{p}{p_0} \right) \quad (\text{dB}) \quad (2)$$

where p is the acoustic pressure and p_0 is the reference sound pressure (= 20×10^{-6} Pa).

2.1.3 Acoustic radiation force

The first process in particle manipulation with sound is an orthokinetic process [16], which is the

acoustic radiation force acting on a particle under a sound pressure field [35]. As the size of particles is much smaller than the wavelength of acoustic wave [36], the acoustic radiation force F_a acting on a small particle can be expressed as [30, 37]:

$$F_a = -(4\pi R^3 / 3) \nabla \left[\frac{P_A^2}{(4\rho_p c_p^2)} \phi_1 - 3\rho_p v_A^2 / 8\phi_2 \right]$$

$$\phi_1 = 1 - \frac{\rho_p c_p^2}{\rho_0 c_0^2} \quad (3)$$

$$\phi_2 = \frac{2(\rho_0 - \rho_p)}{(2\rho_0 + \rho_p)}$$

where R is the equivalent radius of small spherical particles; P_A and v_A are the sound pressure amplitude and the velocity amplitude in acoustic standing waves, respectively; ϕ_1 and ϕ_2 are the acoustic contrast factors; ρ_p and c_p are the density and velocity of the particle, respectively; and ρ_0 and c_0 are the density and speed of sound in the carrier medium, respectively. The Gor'kov equations are applicable to sound pressure fields where a standing wave is sustained [37], but not to the scenarios involving traveling waves.

Under a steady-state condition, particles within a carrier medium (typically air) are influenced by acoustic waves, they can be gathered in sound pressure nodes and anti-nodes [30]. Greenhall et al. [38] used a modified acoustic contrast factor Φ to replace the original acoustic contrast factors ϕ_1 and ϕ_2 , which can be used to identify the attraction of particles at the pressure nodes or anti-nodes. The acoustic contrast factor (Φ) is given by [38, 39]:

$$\Phi = \frac{5\rho_p - 2\rho_0}{2\rho_p + \rho_0} \frac{\beta_p}{\beta_0} \quad (4)$$

where $\beta_p = 1/(\rho_p c_p^2)$ and $\beta_0 = 1/(\rho_0 c_0^2)$ represent the compressibility of the particles and the air carrier medium, respectively. If $\Phi > 0$, particles are driven to the nearest pressure nodes, and if $\Phi < 0$, particles are driven to the nearest pressure anti-nodes [30, 38, 39]. The acoustic contrast factor may be utilized for further analysis of the acoustic radiation force, which generally creates traction on particles within a sound pressure field [40, 41]. Particles may reside in an acoustic pressure antinode with a spatial location where may effectively reduce the particles' velocity as the pressure is maintained.

The second process in particle manipulation with sound involves an aerodynamic mechanism [42], which describes collisions due to viscous interactions between particles and the carrier medium (air). Specifically, this mechanism describes the relationship between the angular velocity of two particles

that may collide within the anti-nodal and nodal locations [43]. This interaction is expressed as follows, which is also called as a secondary radiation force [31, 44-47]:

$$F_s = 4\pi R^6 \left[\overbrace{\frac{(\rho_p - \rho_0)^2 (3 \cos^2 \theta - 1)}{6\rho_0 d^4} v_p^2(x)}^{\text{Particle Velocity Term}} - \overbrace{\frac{\omega^2 \rho_0 (\beta_p - \beta_0)}{9d^2} p_s^2(x)}^{\text{Sound Pressure Term}} \right] \quad (5)$$

and

$$p_s(x) = \frac{P_m}{2} \sin\left(\frac{m\pi x}{L} - 2\pi ft\right) + \frac{P_m}{2} \sin\left(\frac{m\pi x}{L} + 2\pi ft\right) \quad (6)$$

where F_s consists of a particle velocity term and a sound pressure term to represent the particle's trajectory, θ is the angle between the angular velocity from the center of two particles and the propagation direction of an acoustic wave, d is the distance between particles, $v_p(x)$ is the velocity of particles, ω is the angular velocity of the air carrier medium, $p_s(x)$ is the sound pressure, P_m is the peak sound pressure amplitude, x is a spatial variable, and t is a temporal variable.

The effect of the secondary radiation force on a particle entering within the sound pressure field relates to the magnitude of F_s , especially its polarity (represented by a positive or negative number) [44]. If F_s is negative, the interaction between two particles is considered to be attractive, which will promote particle coagulation via a collision process. However, if F_s is positive, the interaction between two particles is repulsive, and thus separation will likely occur as their respective numerical vectors diverge in the localized sound pressure field [45].

2.2 Numerical modelling

Fig. 2 shows a schematic cross-section of the proposed U-shaped acoustic-driven device, with two loudspeakers located at their respective resonance chambers. The reflective panels are positioned in an opposite direction with the loudspeakers to form a standing wave. The chamber contains two airflow inlets and outlets positioned on the lower sides to plug into the ventilation duct. An opening at the sidewall between two chambers allows the airflow to pass from the left chamber to the right one. The overall configuration of the device is treated as a parallel structure, because the generation of sound waves from the loudspeakers is always in an opposite direction of the incoming airflow. The dimensions of the resonance chamber in this study are 10 cm high, 10 cm wide, and 20 cm long. The two chambers are placed in parallel, and thus the overall width is 20 cm. We will simulate the effects of acoustic emission with the loudspeakers to observe the formation of standing waves for a trapping process. Using numerical simulations can identify the trajectories of moving particles under various

airflow rates. To visualize the acoustic-particle interactions and guide the experimental studies, the combined effects of sound pressure and airflow are then investigated to study the particle trajectories.

To simulate the airborne particles motion trajectories under an acoustic treatment, we conduct a numerical analysis using the COMSOL Multiphysics[®] software to investigate the motion of particles driven by acoustic waves. The acoustic pressure model is that of a simplified 2D acoustic enclosure driven at a constant frequency and same phase. To ensure sufficient computational accuracy, meshing is an important descriptor to achieve accurate computational results. Each element edge length is smaller than one-sixth of the wavelength [48-50]. In this model, as the particle diameter (R) is far small compared to the acoustic wavelength (λ), they are modeled as point particles. The condition $R \ll \lambda$ is an important condition for the acoustic radiation force term to be physically correct [51]. Referring to these conditions, an extra-fine meshing is used with a maximum element size of 3 mm [49] and a minimum element size of 0.36 mm.

2.2.1 Governing equations of continuous airflow

Consider the Reynolds-averaged Navier–Stokes (RANS) equations, it is utilized for the present numerical simulation [52, 53]. Using tensor notations, the RANS equations are expressed by [53]

$$\frac{\partial \bar{u}_i}{\partial x_i} = 0 \quad (7)$$

$$\frac{\partial \bar{u}_i}{\partial t} + \bar{u}_j \frac{\partial \bar{u}_i}{\partial x_j} = -\frac{\partial \bar{p}}{\partial x_i} + \nu \frac{\partial^2 \bar{u}_i}{\partial x_j \partial x_j} - \frac{\partial \tau_{ij}}{\partial x_j} \quad (8)$$

where \bar{u}_i is the mean flow velocity, \bar{p} is the mean pressure of a fluid flow, ν is the fluid kinematic viscosity, and τ_{ij} is the Reynolds-stress term. As we mainly focus on the flow patterns and acoustic effects inside the U-shaped device, the boundary conditions of the ventilation duct model are set as a velocity inlet and an arbitrary outlet for numerical analysis.

In addition, a standard k - ε turbulence model [20] can be used to calculate the dynamic viscosity, i.e., $\mu_T = \rho C_\mu k^2 / \varepsilon$ where k denotes the turbulent kinetic energy, and ε denotes the turbulent dissipation rate, and C_μ is a constant ($= 0.09$). The transport equations of this model, in a simple form, can be written as follows [20, 54]

$$\rho_0 \frac{\partial k}{\partial t} + \rho_0 \mathbf{u} \cdot \nabla k = \nabla \cdot \left[\left(\mu_0 + \frac{\mu_T}{\sigma_k} \right) \nabla k \right] + P_k - \rho_0 \varepsilon \quad (9)$$

$$\rho_0 \frac{\partial \varepsilon}{\partial t} + \rho_0 u \cdot \nabla \varepsilon = \nabla \cdot \left[\left(\mu_0 + \frac{\mu_T}{\sigma_\varepsilon} \right) \nabla \varepsilon \right] + C_{\varepsilon 1} \frac{\varepsilon}{k} P_k - C_{\varepsilon 2} \rho_0 \frac{\varepsilon^2}{k} \quad (10)$$

where u is the average flow velocity, ρ_0 is the fluid density, μ_0 is the fluid viscosity, and P_k is the production term. In the above equations, the non-dimensional constants $C_{\varepsilon 1}$, $C_{\varepsilon 2}$, σ_k and σ_ε can be set as 1.44, 1.92, 1.0, and 1.3, respectively. Readers may refer to Refs. [20], [53] and [55] for details.

2.2.2 Dynamic motion of particles under fluid flow

To simplify the numerical model as a 2D model in Fig. 2(a) (i.e., a top view), the motion of particles is investigated with the turbulence model and acoustic model separately. In the turbulence model, we mainly discuss the motion of particles that is affected by a continuous airflow (see Eqs. (7)-(10)). The acoustic effect acting on the released particles is induced by the acoustic radiation force. According to Newton's second law, the motion of particles can be written as [20, 56, 57]

$$\frac{d}{dt}(m_p v) = F_a + F_g + F_d \quad (11)$$

where m_p denotes the particle mass, v denotes the particle velocity, F_g is the gravitational force, and F_d is the drag force. In the equation, F_a is the acoustic force acting on the released particle, we may consider Eq. (4) as aforementioned. The drag force with Ossen's correction [20, 58] can be expressed as follows

$$\begin{aligned} F_d &= \frac{1}{8} C_d \rho_p S |u - v| (u - v) \\ C_d &= \frac{24}{\text{Re}_r} \left(1 + \frac{3}{16} \text{Re}_r \right) \\ \text{Re}_r &= \frac{\rho_0 U_r d_p}{\mu_0} \end{aligned} \quad (12)$$

where C_d is the drag coefficient, Re_r is the relative Reynolds number, U_r is the relative velocity between airflow and particle, ρ_0 is the fluid density, d_p is the particle diameter, ρ_p is the density of particles, μ_0 is the fluid viscosity, and S denotes the projection area of the particle perpendicular to the direction of propagation of acoustic waves.

2.2.3 Initial conditions of numerical simulation

As the dynamic behavior of particles under the action of flow fields and the effect of acoustic radiation force is quite complex, we assume that: (i) the air medium is viscous and incompressible; (ii) the air temperature is constant; (iii) the attenuation of acoustic waves in air is ignored; and (iv) the

particle size is much smaller than the wavelength of acoustic waves. In the numerical model (see Fig. 2(c)), particles are evenly released in the resonant chamber with an initial velocity of 0 m/s. The freeze-wall boundary condition is adopted for each particle, which indicates that the particles would freeze to have an unchanged position and velocity once they touch the chamber wall. We separately simulate the motion of particles by utilizing two models under the airflow and acoustic fields. To illustrate the particle trajectories under the flow field, the RANS equation is utilized to obtain the time-average fluid velocity u . Then, the k - ϵ turbulence model is adopted to consider the turbulence effect within the resonant chambers [20]. To illustrate the motion of particles under an acoustic field, the effect of acoustic radiation force is considered. The drag force induced by the surrounding fluid medium under a static fluid field is considered as well. The operating acoustic frequency inside the U-shaped enclosure can be determined by Eq. (1).

2.3 Device Fabrication and Experiment

To investigate the synergetic effect of particle trapping in the U-shaped design configuration under acoustic fields, we fabricated a prototype to investigate the particle concentration with and without an acoustic force, as shown in Fig. 2(b). We also designed a ventilation duct model coupled by the U-shaped acoustic-driven device for experimental studies, see Figs. 2(d) and 2(e). In this section, we describe the fabrication procedures of the experimental setup to demonstrate and validate the performance of the proposed acoustic-driven device. In the device, we fabricated two resonance chambers by partitioning a cubic transparent acrylic material into two rectangular sections. Two circular sections were cut out of the tube walls in the resonant chambers, and two loudspeakers (*TANBX, TB-412, 4-inch coaxial audio loudspeaker*) were embedded into the circular holes. Stainless-steel sound reflectors were deployed in the opposite direction of the loudspeakers, as shown in Fig. 2(b). The loudspeakers were operated at the same frequency and phase difference, so the occurrence of interference effects would be minimized. In addition, appropriate sealant materials were applied to the acoustic chamber to minimize sound leakage.

A full experimental prototype was constructed to investigate the acoustic effects under various ventilation scenarios, as shown in Figs. 2(d) and 2(e). PM generated by an aerosol generator can be released at the flow inlet, and the particles are allowed to flow into the chamber inlet and through the device to undergo a trapping process. A power supply was connected to the electrical equipment (i.e., power fan, loudspeakers, aerosol generator, and particle size analyzer). Based on the setup, we would

conduct our experiment without a MERV filter to analyze the performance of the acoustic-driven device as a pre-filter, and then test the performance of the setup in combination with a commercial MERV-6-graded filter (*PureFit, Pleated Filter MERV 6 Furnace Filter*). The filtration performance was measured by generating PM aerosols with a particle generator (*TSI, Model 8026*) using a sodium chloride (NaCl) source, and then analyzing their concentration and distribution with a particle size analyzer (*METONE, BT-620*) between 108 and 116 dB. The maximum SPL applied was 116 dB. Airflow was induced with an extraction fan (*APC-10, diameter 100 mm, 2800 r/min, 150 m³/h*) at the tube end, and the fan speed was controlled (between 0.45 and 0.75 m/s) by a controllable frequency inverter circuit. An airflow meter probe (*Testo, Model 435-4*) was used to measure the air velocity at room temperature.

To optimize the filtration efficiency, we analyzed the filtration performance by examining three important parameters. We examined the loudspeaker-operating frequency (that was resonant in the chamber), the applied SPL (dB), and the airflow rate of the ventilation tube under various particle sizes (i.e., 0.3–10 μm) [16]. The efficiency with which a filter removes particles from an airflow represents its effectiveness in reducing the particle concentration within the airflow. Therefore, a removal coefficient that also represents the filtration efficiency (α) is expressed by the following equation [16, 30, 31]:

$$\alpha = \left(\frac{C_1 - C_2}{C_1} \right) \times 100\% \quad (13)$$

where C_1 represents the particle concentration in the absence of the acoustic effect, and C_2 represents the particle concentration in the presence of acoustic effect. We used this equation to determine the overall performance of the device.

3. Results and Discussion

3.1 Numerical analysis

In this study, we performed the numerical investigation of the trapping process in the acoustic resonant chamber. The simulation of sound pressure fields, flow fields and particle trajectories are conducted to visualize the particle trapping process within the acoustic resonant chamber.

Fig. 3 shows a two-dimensional cross-sectional simulation that is used to examine the airflow pathway and the influence of the two-chamber enclosure structure in the absence of acoustic effects. The airflow pathway and speed contour simulated under a steady-state condition within the two

chambers. The boundary condition for the “*flow inlet*” is designated as 0.75 m/s, and the “*flow outlet*” is set at an arbitrary interface. The locations of “*flow inlet*” and “*flow outlet*” are indicated in Fig. 2(c). In these diagrams, there is a significant increase in speed at the gap between two chambers, and at the region near the outlet. Fig. 3(a) shows the profile of flow speed within the U-shaped resonant chambers. Fig. 3(b) presents the trajectory of the airflow with respect to speed. We observe that there is mainly a laminar airflow in the first and second chambers, but a turbulent airflow is also induced at the low velocity regions, due to airflow resistance resulting in the two chambers. Since the pressure nodes have a lower SPL, so particles would be trapped in these regions.

Fig. 4 shows a 2D numerical simulation that consists of two resonance chambers, which was used to investigate the acoustic device. In Fig. 4(a), the sound pressure field region is formed by the sound waves emitted from the loudspeakers at a resonant frequency that corresponds to the dimensions of the chamber. It shows the respective locations of the nodes and anti-nodes, which indicate the highest and lowest SPLs. This creates a pressure differential, resulting in the trapping of particles as they pass from the inlet to the outlet via two sound field regions. Fig. 4(b) presents the variation of sound pressure along the length direction of the resonant chamber at 836 Hz, and Fig. 4(c) shows the trapping of particles at the pressure nodes under acoustic fields.

3.2 Experimental study

Based on the information in Section 3.1, we designed an experimental prototype for verification of this pre-filtering technique by a particle concentration measurement. The filtration of aerosol particles of certain sizes was optimized, to verify the proposed simulation parameters and boundary conditions. The loudspeakers provided specific acoustic pressure waves with a certain dependence on frequency, and we illustrated how this can influence the aerosol concentration of fine particles (0.3–1.0 μm) and coarse particles (2.5–10 μm).

In a preliminary testing, particles were generated by sandpapering balsa wood (*Ochroma pyramidale*; density = 1.16 kg/m^3), and were introduced into the chamber via a sidewall, as it was horizontally oriented. Fig. 5(a) is a resonant particle acoustic pattern under the influence of a standing wave. Figs. 5(b) and 5(c) are enlarged images to show the concentration of particles in the center of the resonance chamber, i.e., the location of the pressure node inside the chamber. It can be seen that the wood powders can be forced and gathered at the center of the resonant tube under 116 dB and 836 Hz. At the pressure node, such powders were aligned to a uniform and multi-line pattern, and the interval between two lines was around 2.43 mm. By adopting this test, it can help reflect the effect of

acoustic force on the lightweight particles under an acoustic field.

To study the acoustic effects, we systematically examined the performance of the device in terms of the reduction in the particle concentration and the removal coefficient, and thereby determined its filtration efficiency. Three case studies were examined to determine the dependence of the device performance on the frequency, SPL, and airflow rate. These parameters are the critical variables to determine the effectiveness of the present device. The findings that support our theoretical simulations of the particle trapping effect are also discussed in this section.

3.2.1 Frequency Dependence on PM Reduction

To examine the frequency dependence on PM reduction in our experiment, we calculated the resonant frequencies of 836, 1637, 2510, 3346, and 4183 Hz under an SPL of 116 dB for the enclosure with a tube length of 10 cm. **The measured particle concentrations, for fine and coarse particles, during the trapping process under various frequencies are presented in Fig. 6.** At 836 Hz (the lowest frequency that was applied), there was a 61% reduction in the particle concentration, which was the strongest trapping effect that was observed. In contrast, at 4183 Hz (the highest frequency that was applied), there was only a 1% reduction in the particle concentration, which was the lowest reduction that was achieved. These data show that acoustic waves in the enclosure induced a significant reduction in particle concentration, and that the greatest reduction occurred at a particle size of 1.0 μm , which is similar to the findings in [31]. This is equal to a removal coefficient of up to 61%. In contrast, the lowest reduction occurred at a particle size of 2.5 μm . This suggests that the particle size resists the trapping effect, due to the influence of the particle velocity and acoustic pressure.

Fig. 6 shows that, under an optimal fundamental resonant frequency of 836 Hz, the reduction in the concentration of fine particles is the highest among others (as shown by the green solid line), and would decrease thereafter, with particles greater than 2.5 μm in size. This trend can also be observed at other resonant frequencies (from 1637 to 4183 Hz) that form a standing wave. However, the particle-reduction trend would decrease when we increased the frequency, as shown by the efficiency of removal of 1.0- μm particles.

3.2.2 SPL Dependence on PM Reduction

In the first case, we determined that 836 Hz was the most effective frequency to promote particle trapping. In the second case, we examined the effects of the SPL on particle reduction. **Fig. 7** shows

the removal coefficient determined for the acoustic-driven device operated at various SPLs. Similar maximum removal coefficients for 1- μm particles were found for SPLs greater than 108 dB. At 108 dB, a linearly increasing trend can be seen as the removal coefficient increases from 3% to 21%, which may indicate insufficiency in the supply of a sound pressure field for the promotion of particle trapping. The maximum removal coefficient for 1- μm particles was again 61%, whereas for $>2.5\text{-}\mu\text{m}$ particles, an SPL of 110 dB increased the removal coefficient from 14% to 34%. Because the removal of finer particles is more difficult, it was optimal to operate the loudspeakers at 116 dB to maximize the trapping effect.

3.2.3 Airflow Dependence on PM Reduction

In this case, we further examined the dependence of acoustic effect on airflow while applying a loudspeaker frequency of 836 Hz at an SPL of 116 dB. Fig. 8 shows the removal coefficient at a flow rate from 0.45 to 0.75 m/s. The results show a maximum removal coefficient trend that is similar to those in Figs. 6 and 7 with respect to the particle size distribution. According to the numerical simulations, it is possible that an increase in the flow rate allows the particle trajectory to provide a recirculating airflow within the chambers and allows particles to reside within the sound pressure field for a longer period. Therefore, as more incoming particles enter into the chamber, the greater airflow can induce a greater recirculating flow within the vertical enclosure and thus cause a greater number of particles to undergo the trapping effect. The results are consistent with the numerical simulation results as shown in Section 3.1.

In Table 1, we summarized the filtration efficiency of particle concentrations under various critical parameters (i.e., frequency, SPL and airflow rate). In addition, a further investigation is presented in the next section to obtain more conclusive data.

3.2.4 Acoustic-based Pre-filtering System

In the previous sections, we analyzed the acoustic effect of the U-shaped device and the optimization of its operating parameters. In this section, we will discuss the improvement provided by the acoustic-driven pre-filter in terms of the overall filtration efficiency. To test and calibrate this device for practical use, we examined the effectiveness of a commercial MERV-6 grade coarse filter when combined with the present technique.

Fig. 9 shows the removal performance pertaining to a MERV-6 coarse filter, the present technique,

and a MERV-6 filter combined with the present technique. The MERV-6 filter achieved an average reduction in the concentration for coarse particles ($>2.5 \mu\text{m}$) of 50%, corresponding to the *PureFit Pleated Filter* specifications (i.e., a filtration efficiency up to 60% for $0.3\text{--}10.0 \mu\text{m}$ particles). However, the filtration performance of the MERV-6 filter considerably decreased for particles smaller than $1.0 \mu\text{m}$, which was expected. Therefore, significantly improved filtration performance can be obtained when the MERV-6 filter was used in combination with the acoustic-driven pre-filtering technique. Furthermore, the acoustic-based pre-filtration technique can compensate for the ineffective fine-particle removal rate by the MERV-6 filter, resulting in a maximum removal coefficient of up to 89%. If the MERV-6 filter was absent, the present technique can still achieve a maximum removal coefficient of up to 61% efficiency for particle sizes approaching $1.0 \mu\text{m}$. These data indicate that the present pre-filtering technique is more effective to remove fine particles than coarse particles. Therefore, an acoustic-based pre-filtration technique complements MERV-6 filters can be designed for the removal of fine particles. This also shows that the combination of the present technique with MERV-6 filters may generate a cost effectiveness and long-use filtration device.

To benchmark our results with those in the literature, Fig. 10 depicts the filtration efficiency for the present pre-filtering technique combined with a low-grade MERV-6 filter for comparison. To demonstrate the working performance, we selected a common HVAC filter (MERV-6 filter) for analysis. Our device achieved a high performance of up to 89% efficiency, which indicates that it is an effective method for the removal of fine particles. Notably, our device was more than 100% better for filtering $0.3\text{--}2.0 \mu\text{m}$ particles than cabin filters, which are often implemented in vehicle-based applications [59]. Compared to the high-grade MERV-13 filter as tested by Dols et al. [60], our achieved efficiency was also consistent with the MERV-13 filter for a particle size of $0.4\text{--}1.0 \mu\text{m}$. This finding indicates that if a MERV-6 graded filter is replaced with high-grade filters, the filtration performance will be further increased, without the need to rely solely on very high-performance-based HEPA-type filters. Compared to the fine-particle filter (F6-class) [61], our device can present a better removal efficiency rate at a region of $0.3\text{--}1.0 \mu\text{m}$. Notably, our device also exhibited better performance than those low-grade HVAC filters [62]. The removal efficiency of the present technique would decrease when the particle size is larger than $1.0 \mu\text{m}$ due to the interaction of acoustic strength. In reality, it is rather difficult to filter the sub-micron particles than the super-micron particles, the present filtration technique provides an effective avenue for this issue.

In addition to indoor air quality, it is known that reducing airborne transmission of virus in enclosed areas requires effective control measures, including ventilation and air filtration [3]. Recent

epidemiological studies [63] indicated that aerosol transmission of SARS-CoV-2 mainly includes two size ranges, one is in the sub-micron range (0.25–1.0 μm) and the other one is in the super-micron range ($> 2.5 \mu\text{m}$). The study presented herein shows good results for the sub-micron range (0.3–1.0 μm). Hence, the potential application of this engineering design is a promising approach to reduce the possibility of airborne viral transmission in ventilated indoor spaces. Although HEPA filters can provide high-performance protection for contamination control, this inevitably induces greater extraction fan power in a ventilation system to maintain the required flow rate. The present investigation also provides insights into the improved design of a non-invasive pre-filtering approach in ventilation systems, as the design possesses a high level of flexibility to work with various filter types.

4. Conclusions

The implementation of an acoustic-based manipulation device can achieve a high-efficiency particulate air filter without sacrificing much desired airflow inside mechanical ventilation systems. The major findings of this work are summarized as follows:

- A simple U-shaped acoustic-driven resonating device that can greatly enhance the filtration rate of low-grade filters for the sub-micron particles (0.3–1.0 μm) under a lower SPL has been proposed.
- To facilitate the trapping effect inside the resonant chambers, loudspeakers were deployed at the sidewall positions, where the generation of acoustic waves is in an opposite direction against an incoming airflow.
- To verify the proposed technique, a prototype was fabricated and experimental tests were conducted to investigate the extent of trapping fine particles with various sizes. Parametric studies of the device performance on acoustic frequency, SPL and flow speed were investigated. As a standalone device, it can achieve a filtration efficiency of 61% and operate at a far lower SPL (116 dB) than those reported in the literature.
- Coupling with a MERV-6 graded coarse filter, the acoustic effect could reduce the presence of particles at the sub-micron range of 0.3–1.0 μm , with up to 89% efficiency for the removal coefficient of 1.0- μm particles. The removal efficiency can be flexibly enhanced by coupling the present design with high-grade filters.

Although this work is not on the morphological and interactive properties of sub-micron particles,

the present design has shown good potential to perform as an effective air-cleaning strategy in mechanically ventilated systems. It is expected to bring better resource efficiency for maintaining a healthy and pleasant built environment. In the future work, a refined study will focus on the microscopic interactions in the pressure node regions, the influence of greater airflow rates on the working efficiency, and the sensitivity of acoustic frequencies on various particle sizes.

Acknowledgements

The work described in this paper was supported by the General Research Fund from the Research Grants Council of the Hong Kong Special Administrative Region (Project No. 152008/19E). In addition, the authors would also like to express our sincere appreciation and gratitude to the support of the Fire Engineering Laboratory at Department of Building Services Engineering, The Hong Kong Polytechnic University.

References:

- [1] I. Manisalidis, E. Stavropoulou, A. Stavropoulos *et al.*, (2020) "Environmental and Health Impacts of Air Pollution: A Review," *Frontiers in Public Health*, vol. 8, no. 14.
- [2] J. J. K. Jaakkola, L. M. Reinikainen, O. P. Heinonen *et al.*, (1991) "Indoor air quality requirements for healthy office buildings: Recommendations based on an epidemiologic study," *Environment International*, vol. 17, no. 4, pp. 371-378.
- [3] L. Morawska, J. W. Tang, W. Bahnfleth *et al.*, (2020) "How can airborne transmission of COVID-19 indoors be minimised?," *Environ Int*, vol. 142, 105832.
- [4] H. Qian, T. Miao, L. Liu *et al.*, (2020) "Indoor transmission of SARS-CoV-2," *Indoor Air*.
- [5] Y. Li, G. M. Leung, J. W. Tang *et al.*, (2007) "Role of ventilation in airborne transmission of infectious agents in the built environment - a multidisciplinary systematic review," *Indoor Air*, vol. 17, no. 1, pp. 2-18.
- [6] K. Khankari, (2016) "Patient room HVAC: Airflow path matters," *ASHRAE Journal*, vol. 58, pp. 16-26.
- [7] H. Qian, Y. Li, P. V. Nielsen *et al.*, (2006) "Dispersion of exhaled droplet nuclei in a two-bed hospital ward with three different ventilation systems," *Indoor Air*, vol. 16, no. 2, pp. 111-28.
- [8] H. Sha and D. Qi, (2020) "A Review of High-Rise Ventilation for Energy Efficiency and Safety," *Sustainable Cities and Society*, vol. 54, no. 101971.
- [9] G. Liu, M. Xiao, X. Zhang *et al.*, (2017) "A review of air filtration technologies for sustainable and healthy building ventilation," *Sustainable Cities and Society*, vol. 32, pp. 375-396.
- [10] D. Kim and S. J. Lee, (2020) "Effect of water microdroplet size on the removal of indoor particulate matter," *Building and Environment*, vol. 181, no. 107097.
- [11] A. C. Veeck, (2008) "Air filtration: Guidelines and standards for using air filters," *Filtration & Separation*, vol. 45, no. 1, pp. 28-30.
- [12] M. Evander and T. Laurell, "Acoustic Trapping," in *Encyclopedia of Nanotechnology*, B. Bhushan Ed. Dordrecht: Springer Netherlands, 2012, pp. 41-45.
- [13] E. H. Brandt, (2001) "Suspended by sound," *Nature*, vol. 413, no. 6855, pp. 474-475.
- [14] S. Temkin, (1994) "Gasdynamic agglomeration of aerosols. I. Acoustic waves," *Physics of Fluids*, vol. 6, no. 7, pp. 2294-2303.
- [15] T. L. Hoffmann, (2000) "Environmental implications of acoustic aerosol agglomeration," *Ultrasonics*, vol. 38, no. 1, pp. 353-357.
- [16] B. F. Ng, J. W. Xiong, and M. P. Wan, (2017) "Application of acoustic agglomeration to enhance air filtration efficiency in air-conditioning and mechanical ventilation (ACMV) systems," *PLOS ONE*, vol. 12, no. 6.
- [17] E. Riera-Franco de Sarabia and J. A. Gallego-Juárez, (1986) "Ultrasonic agglomeration of micron aerosols under standing wave conditions," *Journal of Sound and Vibration*, vol. 110, no. 3, pp. 413-427.
- [18] S.-C. Fu, W.-T. Yuen, C. Wu *et al.*, (2015) "Finite-difference lattice Boltzmann simulation on acoustics-induced particle deposition," *Comptes Rendus Mécanique*, vol. 343, no. 10, pp. 589-598.
- [19] J. Liu and X. Li, (2020) "A computational investigation of particle acoustic agglomeration in a resonance tube," *Powder Technology*, vol. 374, pp. 82-94.
- [20] Y. Shi, J. Wei, W. Bai *et al.*, (2020) "Numerical investigations of acoustic agglomeration of liquid

- droplet using a coupled CFD-DEM model," *Advanced Powder Technology*, vol. 31, no. 6, pp. 2394-2411.
- [21] Y. Shi, J. Wei, J. Qiu *et al.*, (2020) "Numerical study of acoustic agglomeration process of droplet aerosol using a three-dimensional CFD-DEM coupled model," *Powder Technology*, vol. 362, pp. 37-53.
- [22] J. Zheng, Y. Li, Z. Wan *et al.*, (2019) "Modification of the agglomeration kernel and simulation of the flow pattern in acoustic field with fine particles," *Powder Technology*, vol. 356, pp. 930-940.
- [23] E. N. da C. Andrade, (1936) "The coagulation of smoke by supersonic vibrations," *Transactions of the Faraday Society*, vol. 32, no. 0, pp. 1111-1115.
- [24] H. W. S. Clair, (1949) "Agglomeration of Smoke, Fog, or Dust Particles by Sonic Waves," *Industrial & Engineering Chemistry*, vol. 41, no. 11, pp. 2434-2438.
- [25] E. P. Mednikov, "Acoustic Coagulation and Precipitation of Aerosols: Authorized Translation from the Russian by Chas. V. Larrick". Consultants Bureau, 1965.
- [26] W. T. Yuen, S. C. Fu, and C. Y. H. Chao, (2016) "The correlation between acoustic streaming patterns and aerosol removal efficiencies in an acoustic aerosol removal system," *Aerosol Science and Technology*, vol. 50, no. 1, pp. 52-62.
- [27] W. T. Yuen, S. C. Fu, J. K. C. Kwan *et al.*, (2014) "The Use of Nonlinear Acoustics as an Energy-Efficient Technique for Aerosol Removal," *Aerosol Science and Technology*, vol. 48, no. 9, pp. 907-915.
- [28] W. T. Yuen, S. C. Fu, and Christopher Y. H. Chao, (2017) "The effect of aerosol size distribution and concentration on the removal efficiency of an acoustic aerosol removal system," *Journal of Aerosol Science*, vol. 104, pp. 79-89.
- [29] C.-h. Shi, J. Zhang, Y. Zhao *et al.*, (2017) "Acoustic Agglomeration Process of Fine Particles in a Resonance Structure," *IOP Conference Series: Earth and Environmental Science*, vol. 78.
- [30] Z. Qiao, Y. Huang, N. Vincenzo *et al.*, (2015) "Aerosol manipulation by acoustic tunable phase-control at resonant frequency," *Powder Technology*, vol. 281, pp. 76-82.
- [31] Z. Qiao, Y. Huang, N. Vincenzo *et al.*, (2017) "Aerosol manipulation through modulated multiple acoustic wavepackets with a pair of resonators," *Powder Technology*, vol. 322, pp. 24-31.
- [32] S.K. Lai, Y.T. Zhang, J.C.W. Yu *et al.*, "A new approach for an induced coagulation of particulate matter through thermo-acoustic agglomeration," in *Proceedings of Inter-Noise 2020 E-Congress*, Seoul, Korea, 23-26 Aug 2020,
- [33] G. Zhang, J. Wang, Z. Chi *et al.*, (2018) "Acoustic agglomeration with addition of sprayed liquid droplets: Three-dimensional discrete element modeling and experimental verification," *Chemical Engineering Science*, vol. 187, pp. 342-353.
- [34] J. A. Gallego-Juárez, E. Riera-Franco De Sarabia, G. Rodríguez-Corral *et al.*, (1999) "Application of Acoustic Agglomeration to Reduce Fine Particle Emissions from Coal Combustion Plants," *Environmental Science & Technology*, vol. 33, no. 21, pp. 3843-3849.
- [35] K. Yasui, "Fundamentals of Acoustic Cavitation and Sonochemistry," in *Theoretical and Experimental Sonochemistry Involving Inorganic Systems*, M. Ashokkumar Ed. Dordrecht: Springer Netherlands, 2011, pp. 1-29.
- [36] D. Foresti, M. Nabavi, and D. Poulikakos, (2012) "On the acoustic levitation stability behaviour of spherical and ellipsoidal particles," *Journal of Fluid Mechanics*, vol. 709, pp. 581-592.
- [37] L. P. Gor'kov, (1962) "On the Forces Acting on a Small Particle in an Acoustical Field in an Ideal

Fluid," Soviet Physics Doklady, vol. 6, 773.

- [38] J. Greenhall, F. Guevara Vasquez, and B. Raeymaekers, (2013) "Continuous and unconstrained manipulation of micro-particles using phase-control of bulk acoustic waves," Applied Physics Letters, vol. 103, no. 7, 074103.
- [39] D. Karpul, J. Tapson, M. Rapson *et al.*, (2010) "Limiting factors in acoustic separation of carbon particles in air," The Journal of the Acoustical Society of America, vol. 127, no. 4, pp. 2153-2158.
- [40] R. Habibi, C. Devendran, and A. Neild, (2017) "Trapping and patterning of large particles and cells in a 1D ultrasonic standing wave," Lab on a Chip, vol. 17, no. 19, pp. 3279-3290.
- [41] A. Haake and J. Dual, (2002) "Micro-manipulation of small particles by node position control of an ultrasonic standing wave," Ultrasonics, vol. 40, no. 1, pp. 317-322.
- [42] I. a. González, J. A. Gallego-Juárez, and E. Riera, (2003) "The influence of entrainment on acoustically induced interactions between aerosol particles—an experimental study," Journal of Aerosol Science, vol. 34, no. 12, pp. 1611-1631.
- [43] D. Saeidi, M. Saghafian, S. Haghjooy Javanmard *et al.*, (2020) "A Quantitative Study of the Secondary Acoustic Radiation Force on Biological Cells during Acoustophoresis," Micromachines (Basel), vol. 11, no. 2, 152.
- [44] E. Benes, M. Groschl, H. Nowotny *et al.*, "Ultrasonic separation of suspended particles". 2001, pp. 649-659.
- [45] M. Weiser, R. Apfel, and E. Neppiras, (1984) "Interparticle force on red-cells in a standing wave field," Acta Acustica united with Acustica, vol. 56, no. 2.
- [46] K. H. Ahn, J. Ahn, I. T. Kim *et al.*, (2015) "Separation of fine particles at different frequencies and HRTs using acoustic standing waves," Environ Technol, vol. 36, no. 1-4, pp. 302-9.
- [47] T. Laurell, F. Petersson, and A. Nilsson, (2007) "Chip integrated strategies for acoustic separation and manipulation of cells and particles," Chem Soc Rev, vol. 36, no. 3, pp. 492-506.
- [48] P. B. Muller, R. Barnkob, M. J. H. Jensen *et al.*, (2012) "A numerical study of microparticle acoustophoresis driven by acoustic radiation forces and streaming-induced drag forces," Lab on a Chip, vol. 12, no. 22, pp. 4617-4627.
- [49] V. Rokad and D. H. Pandya, (2020) "Development of 3D improved acoustic transient model for vibro cleaner using COMSOL multiphysics," Materials Today: Proceedings.
- [50] X. Peng, W. He, F. Xin *et al.*, (2020) "The acoustic radiation force of a focused ultrasound beam on a suspended eukaryotic cell," Ultrasonics, vol. 108, no. 106205.
- [51] H. Bruus, (2012) "Acoustofluidics 7: The acoustic radiation force on small particles," LAB CHIP, vol. 12, no. 6, pp. 1014-121.
- [52] D. C. Wilcox, "Turbulence modeling for CFD," 2nd ed. La Cañada, Calif.: DCW Industries, 2000.
- [53] G. Alfonsi, (2009) "Reynolds-Averaged Navier-Stokes Equations for Turbulence Modeling," Applied Mechanics Reviews, vol. 62.
- [54] W. Rodi, "Turbulence Models and Their Application in Hydraulics". Pennsylvania, USA: Routledge Press, 2017.
- [55] D. C. Wilcox, "Turbulence Modeling for CFD ". California, USA: DCW Industries 1998.
- [56] R. Kačianauskas, V. Rimša, A. Kačeniauskas *et al.*, (2018) "Comparative DEM-CFD study of binary interaction and acoustic agglomeration of aerosol microparticles at low frequencies," Chemical Engineering Research and Design, vol. 136, pp. 548-563.
- [57] M.-m. Kim and A. L. Zydney, (2004) "Effect of electrostatic, hydrodynamic, and Brownian forces on particle trajectories and sieving in normal flow filtration," Journal of Colloid and Interface

Science, vol. 269, no. 2, pp. 425-431.

- [58] C. W. Oseen, (1910) "Über die Stokes' sche Formel und Über eine verwandte Aufgabe in der Hydrodynamik," *Ark. Mat. Astron. Fysik.*, vol. 9, pp. 1–20.
- [59] B. Xu, S. Liu, J. Liu *et al.*, (2011) "Effects of Vehicle Cabin Filter Efficiency on Ultrafine Particle Concentration Ratios Measured In-Cabin and On-Roadway," *Aerosol Science and Technology*, vol. 45, no. 2, pp. 234-243.
- [60] W. Dols, B. Polidoro, D. Poppendieck *et al.*, "A Tool to Model the Fate and Transport of Indoor Microbiological Aerosols (FaTIMA)". 2020.
- [61] B. Zhao, N. An, and C. Chen, (2020) "Using air purifier as a supplementary protective measure in dental clinics during the COVID-19 pandemic," *Infection Control and Hospital Epidemiology*.
- [62] National Institute for Occupational Safety and Health, "Guidance for filtration and air-cleaning systems to protect building environments from protect building environments from airborne chemical, biological, or radiological attacks," *DHHS (NIOSH) Publication Number 2003-136*, 2003.
- [63] Y. Liu, Z. Ning, Y. Chen *et al.*, (2020) "Aerodynamic analysis of SARS-CoV-2 in two Wuhan hospitals," *Nature*, vol. 582, no. 7813, pp. 557-560.

Caption of Table:

Table 1. Filtration efficiency of particle concentrations under various parameters.

Captions of Figures:

Fig. 1. Illustration of aerosol particulate transport under the acoustic effects: (a) a loudspeaker is mounted at the top of a ventilation duct; (b) a loudspeaker is mounted at the sidewall of a ventilation duct (present design).

Fig. 2.(a) Schematic diagram (top view) of the U-shaped acoustic-driven device; (b) Photo of the fabricated acoustic-driven device (top view); (c) Schematic diagram of a ventilation duct with the U-shaped acoustic-driven device (top view); (d) Experimental setup (side view) of a ventilation tube with the U-shaped acoustic-driven device; and (e) Experimental setup (top view) comprises of an aerosol source, a trapping zone, a MERV commercial filter (*PureFit, Pleated Filter MERV 6 Furnace Filter*) and a power fan.

Fig. 3. A 2D numerical simulation: (a) the airflow speed contour map under a steady-state condition; and (b) the particle trajectory of a laminar flow occurs within the chambers with a minimal airflow resistance.

Fig. 4. A 2D numerical simulation of the device operating at 836 Hz and 116 dB. (a) Formations of a standing wave and a pressure differential (at 10 cm location) to facilitate particle trapping; (b) Variation of sound pressure along the length direction of the resonant chambers at 836 Hz; and (c) Trapping of particles at the pressure nodes.

Fig. 5. Preliminary test of wood powders generated from sandpapering balsa wood (*Ochroma pyramidale*; density = 1.16 kg/m³): (a) Balza wood within the resonant chamber under 116 dB and 836 Hz; (b) Particles concentrated at the pressure node; and (c) A multi-line pattern of wood powders under standing waves within the resonant chamber.

Fig. 6. Removal coefficient of particles under various resonant frequencies (between 836 Hz and 4183 Hz) at 116 dB.

Fig. 7. Removal coefficient of particles at 836 Hz under various SPLs.

Fig. 8. Removal coefficient of particles under the inlet flow speed of 0.45–0.75 m/s.

Fig. 9. Filtration efficiency of a MERV-6 filter (green dash line), present technique (blue dash line), and a MERV filter with the present technique (red solid line).

Fig. 10. Performance comparison between MERV-6 filter coupling with the present U-shaped device, cabin filter [59], MERV-13 filter [60], fine filter (F6 class) [61], and low-grade filter (35–45% and 60–65%) [62].

Table 1. Filtration efficiency of particle concentrations under various parameters

Under various operating frequencies			
Operating Frequency	Operating SPL	Inlet flow speed	Removal coefficient for PM 1.0
836 Hz	116 dB	0.75 m/s	61.4%
1637 Hz			46.1%
2510 Hz			37.3%
3346 Hz			30.7%
4183 Hz			30.6%

Under various SPLs			
Operating Frequency	Operating SPL	Inlet flow speed	Removal efficiency for PM 1.0
836 Hz	116 dB	0.75 m/s	61.4%
	114 dB		51.7%
	112 dB		30.3%
	110 dB		26.7%
	108 dB		6.8%

Under various inlet flow conditions			
Operating Frequency	Operating SPL	Inlet flow speed	Removal efficiency for PM 1.0
836 Hz	116 dB	0.75 m/s	61.4%
		0.6 m/s	42.8%
		0.5 m/s	43.0%
		0.45 m/s	47.0%

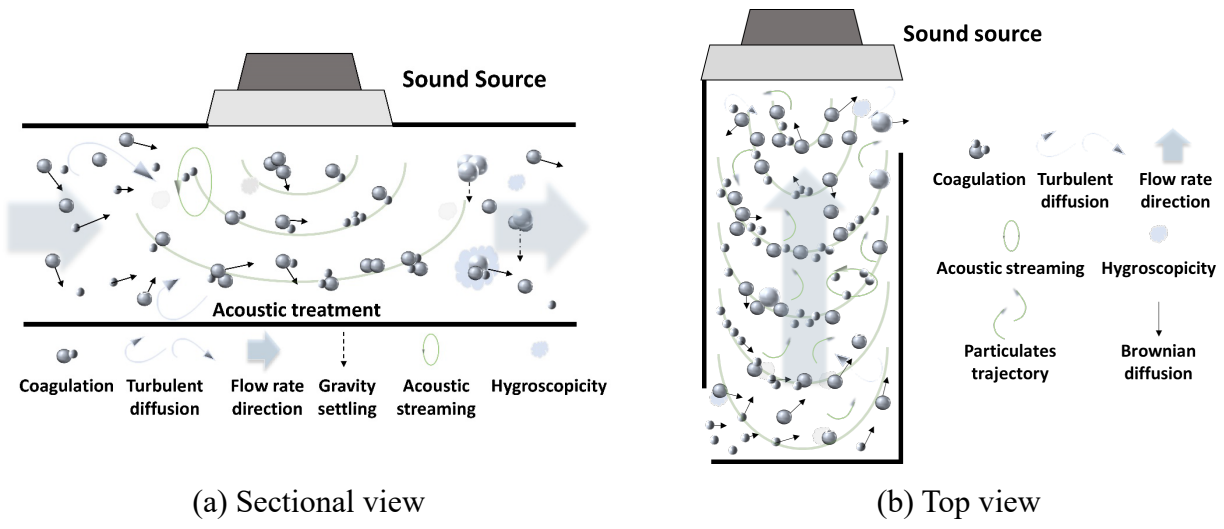


Fig. 1. Illustration of aerosol particulate transport under the acoustic effects: (a) a loudspeaker is mounted at the top of a ventilation duct; (b) a loudspeaker is mounted at the sidewall of a ventilation duct (present design).

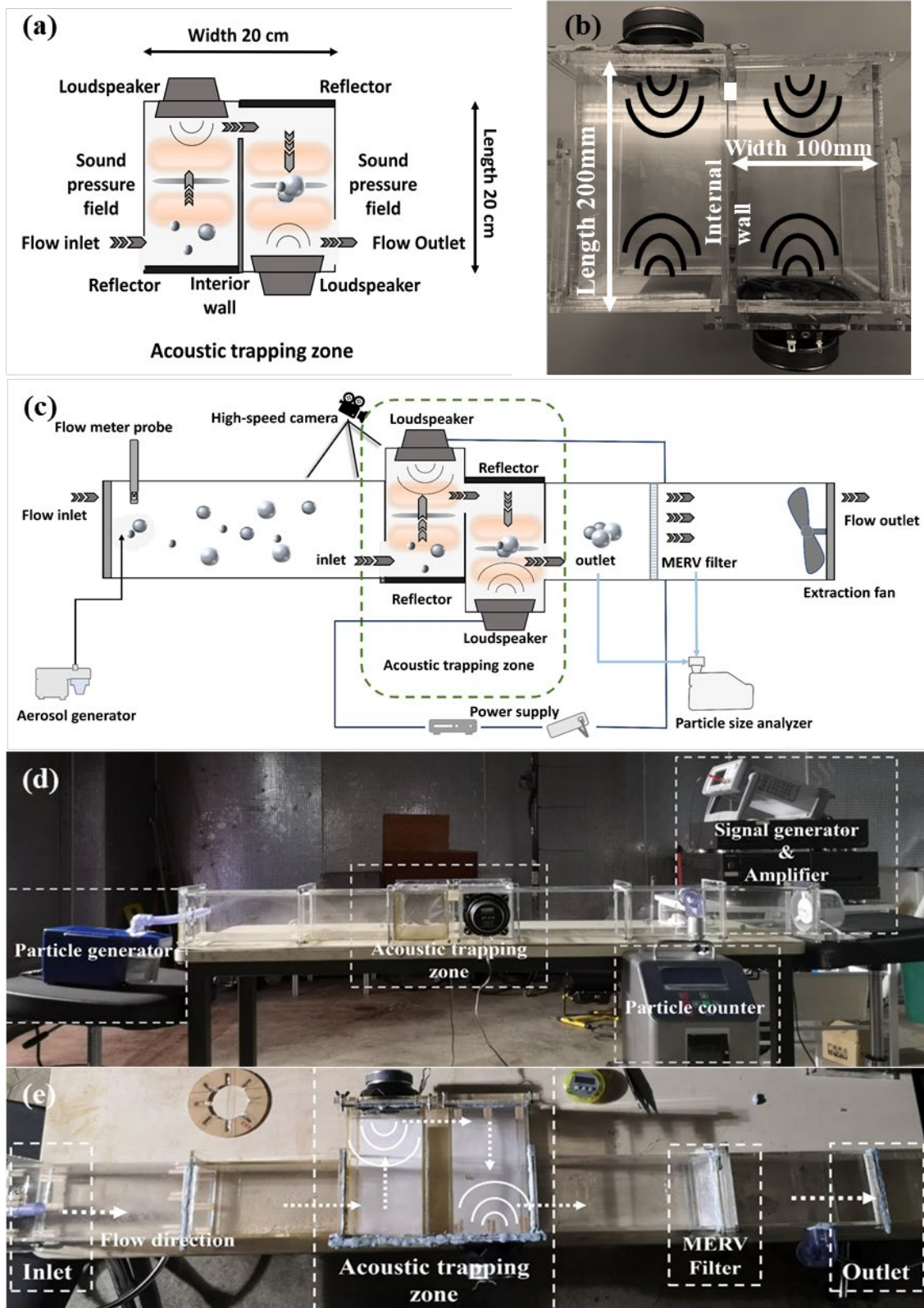


Fig. 2.(a) Schematic diagram (top view) of the U-shaped acoustic-driven device; (b) Photo of the fabricated acoustic-driven device (top view); (c) Schematic diagram of a ventilation duct with the U-shaped acoustic-driven device (top view); (d) Experimental setup (side view) of a ventilation tube with the U-shaped acoustic-driven device; and (e) Experimental setup (top view) comprises of an aerosol source, a trapping zone, a MERV commercial filter (*PureFit, Pleated Filter MERV 6 Furnace Filter*) and a power fan.

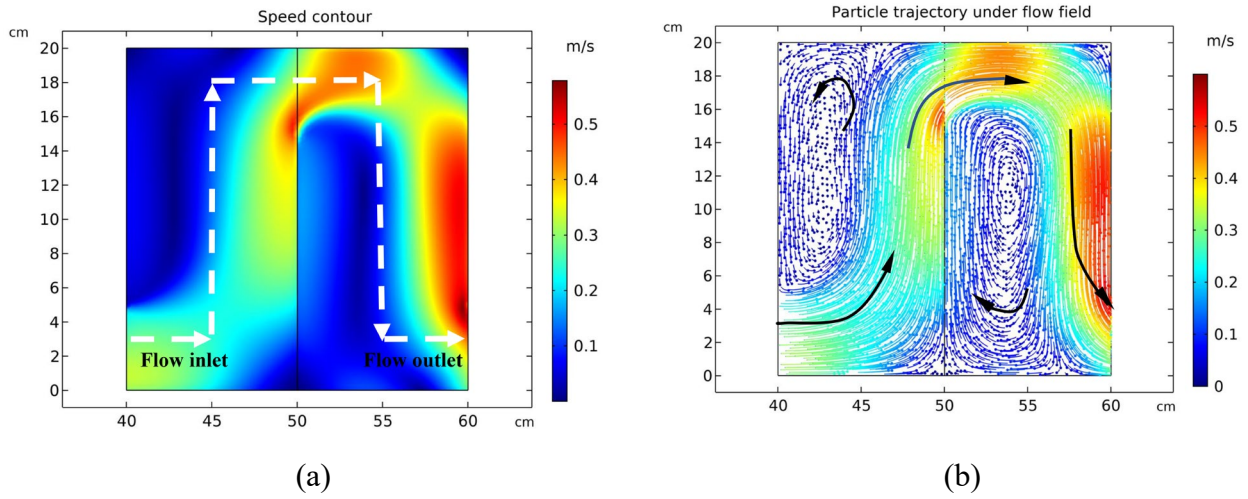


Fig. 3. A 2D numerical simulation: (a) the airflow speed contour map under a steady-state condition; and (b) the particle trajectory of a laminar flow occurs within the chambers with a minimal airflow resistance.

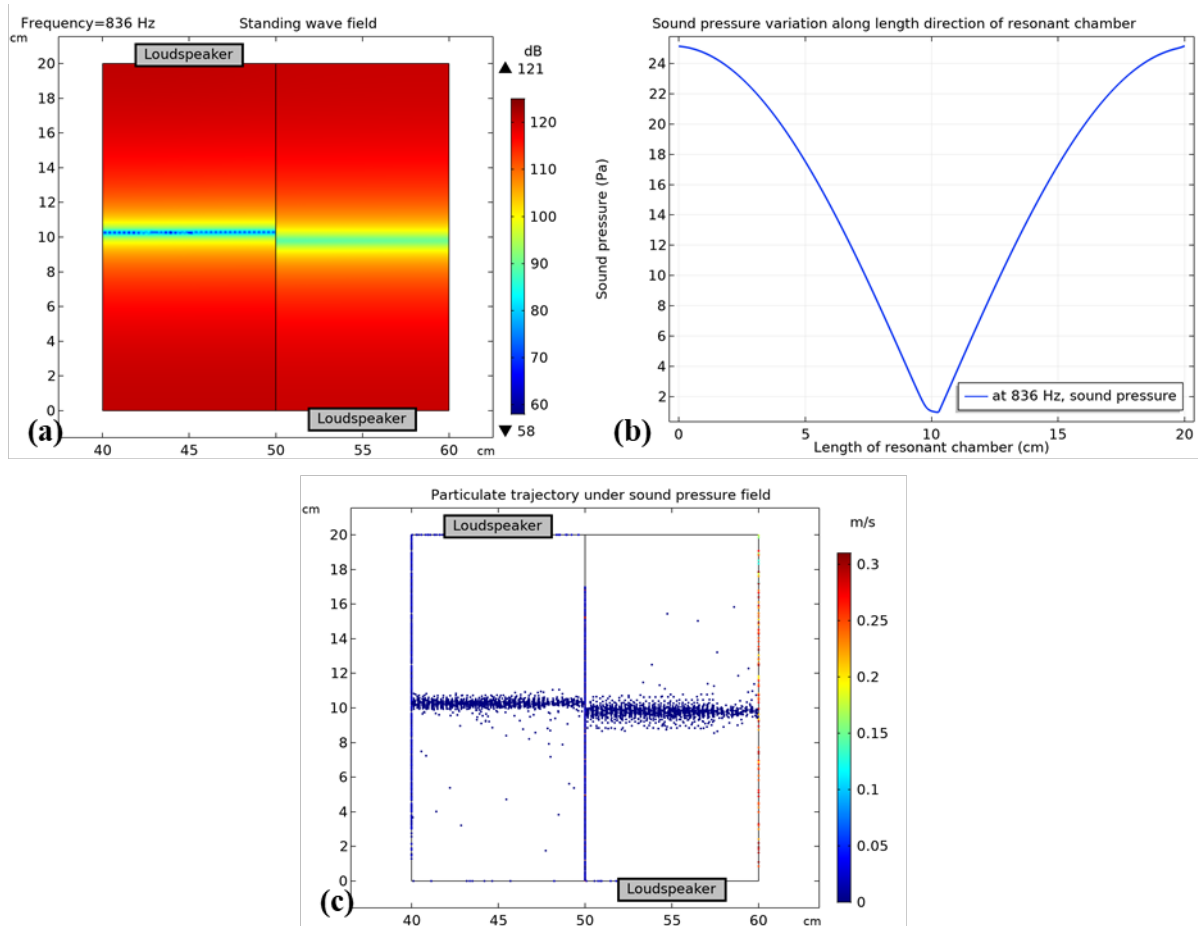


Fig. 4. A 2D numerical simulation of the device operating at 836 Hz and 116 dB. (a) Formations of a standing wave and a pressure differential (at 10 cm location) to facilitate particle trapping; (b) Variation of sound pressure along the length direction of the resonant chambers at 836 Hz; and (c) Trapping of particles at the pressure nodes.

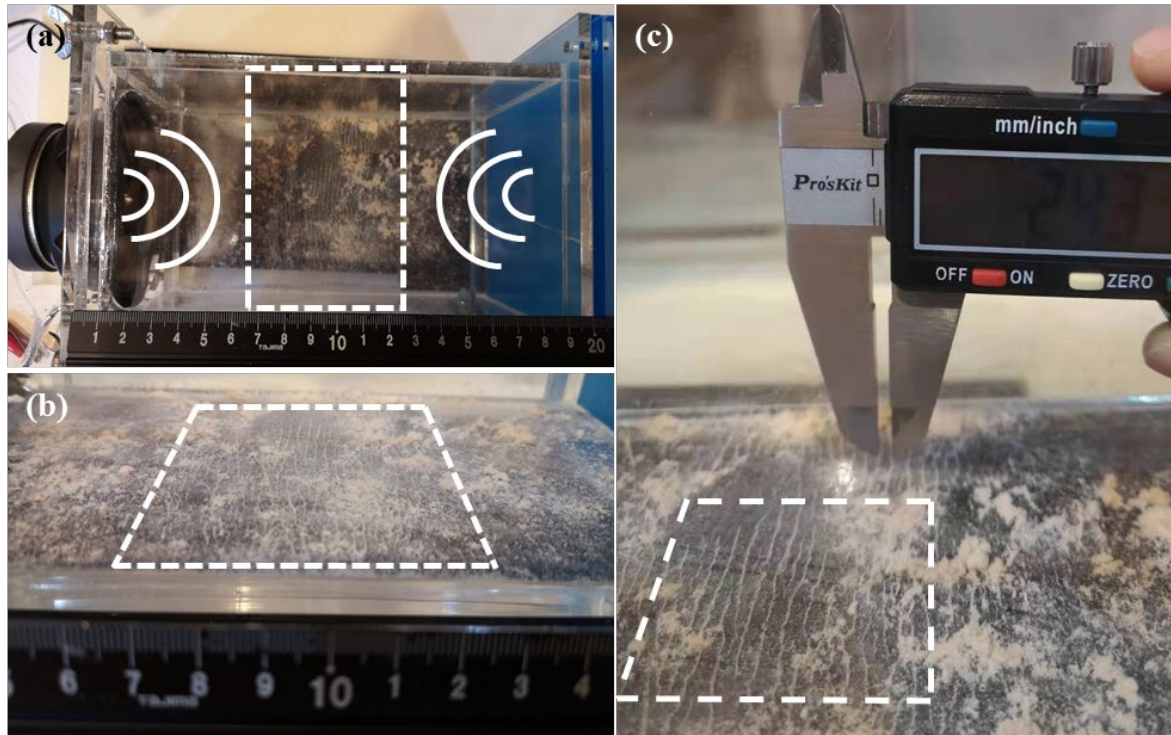


Fig. 5. Preliminary test of wood powders generated from sandpapering balsa wood (*Ochroma pyramidale*; density = 1.16 kg/m^3): (a) Balza wood within the resonant chamber under 116 dB and 836 Hz; (b) Particles concentrated at the pressure node; and (c) A multi-line pattern of wood powders under standing waves within the resonant chamber.

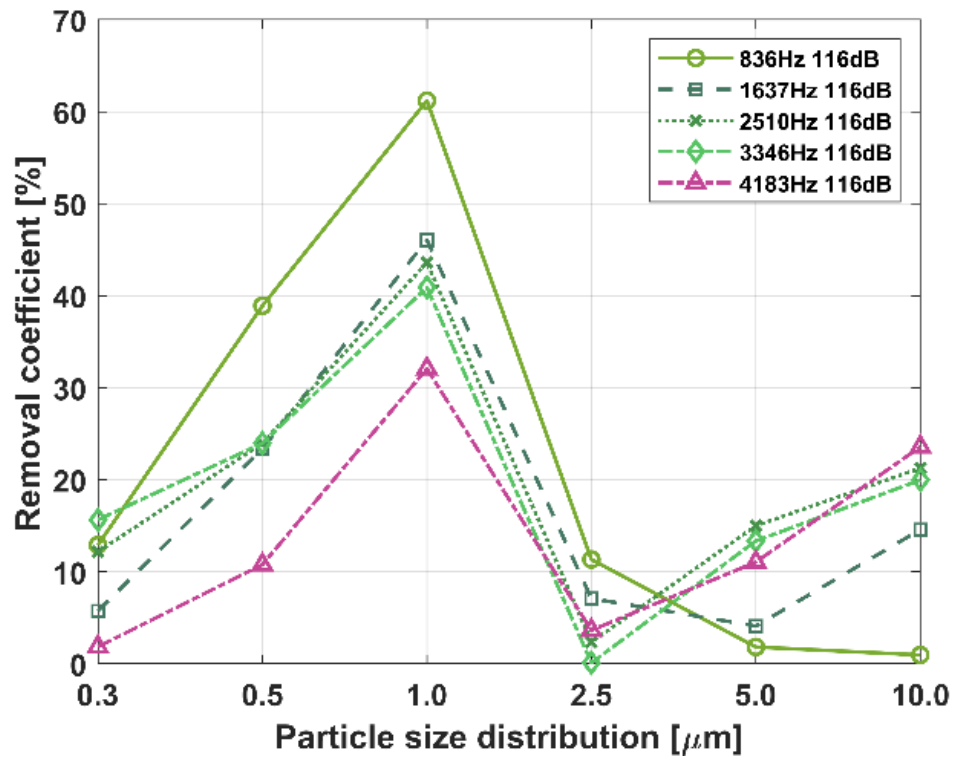


Fig. 6. Removal coefficient of particles under various resonant frequencies (between 836 Hz and 4183 Hz) at 116 dB.

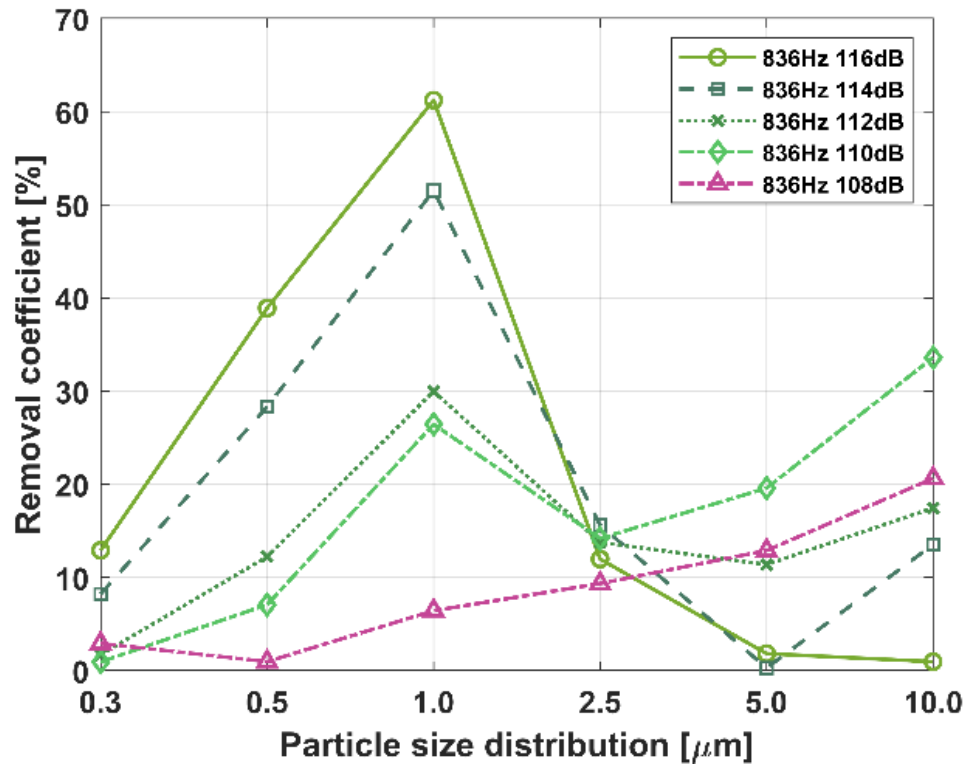


Fig. 7. Removal coefficient of particles at 836 Hz under various SPLs.

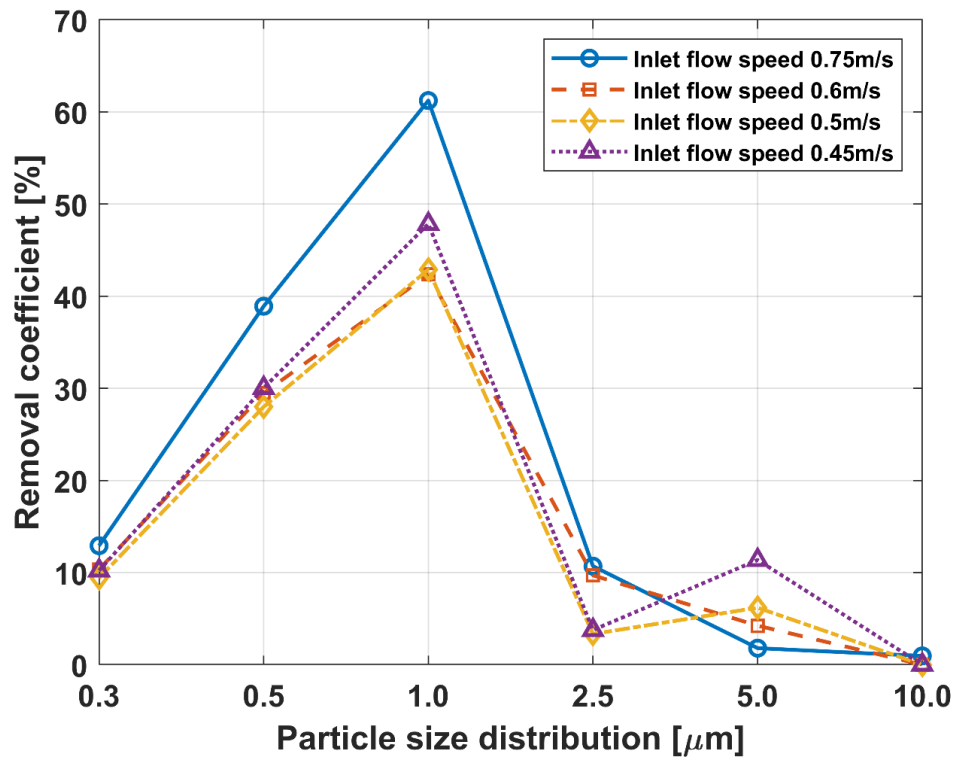


Fig. 8. Removal coefficient of particles under the inlet flow speed of 0.45–0.75 m/s.

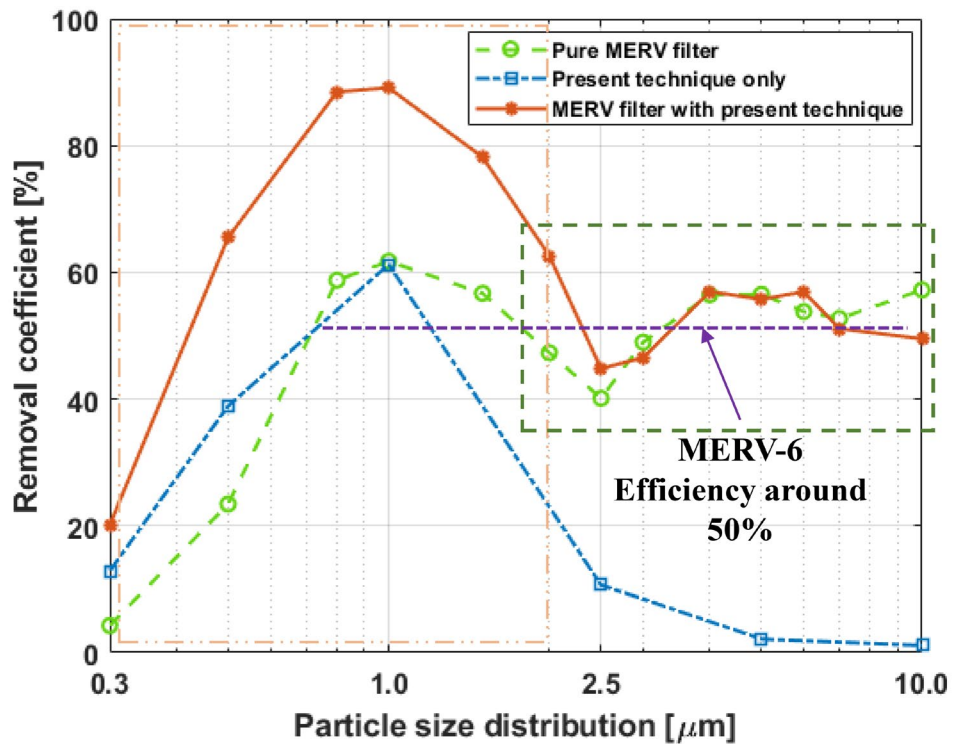


Fig. 9. Filtration efficiency of a MERV-6 filter (green dash line), present technique (blue dash line), and a MERV filter with the present technique (red solid line).

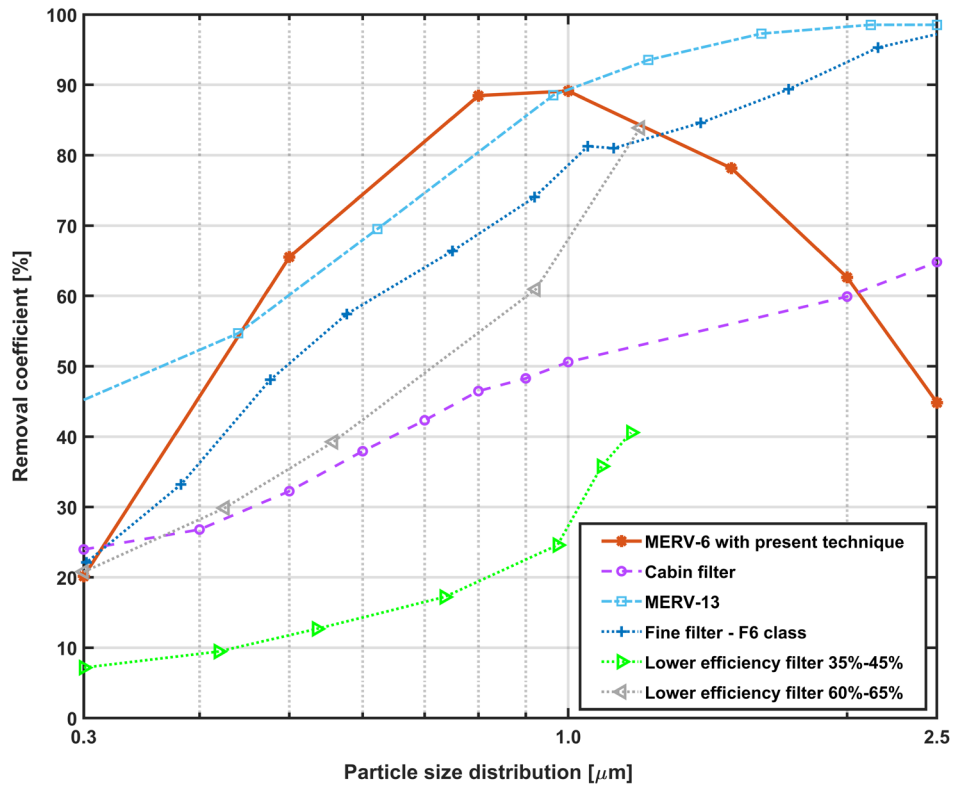


Fig. 10. Performance comparison between MERV-6 filter coupling with the present U-shaped device, cabin filter [59], MERV-13 filter [60], fine filter (F6 class) [61], and low-grade filter (35–45% and 60–65%) [62].